Colloids and Surfaces A: Physicochem. Eng. Aspects 408 (2012) 71–78

Contents lists available at SciVerse ScienceDirect

Colloids and Surfaces A: Physicochemical and Engineering Aspects

journal homepage: www.elsevier.com/locate/colsurfa

Alignment of layered double hydroxide platelets

Yan Zhang, Julian R.G. Evans*

Department of Chemistry, University College London, 20 Gordon Street, London WC1H 0AJ, UK

HIGHLIGHTS

- LDH tactoids were synthesized in stable and flocculating suspensions.
- Highly ordered planar random structures were made by filtration.
- In flocculating systems, edge-face interactions are overcome during filtration.
- Exfoliated LDH suspensions also assembled as rippled layered structures.
- These assemblies prepare for large-scale assembly of nacre-like nanocomposites.

GRAPHICAL ABSTRACT

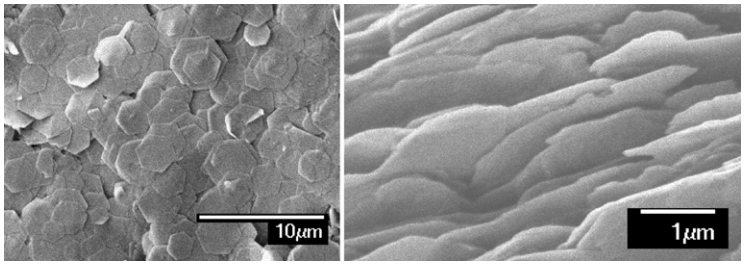

ARTICLE INFO

Article history:
Received 15 March 2012
Received in revised form 15 May 2012
Accepted 19 May 2012
Available online 2 June 2012

Keywords:
Layered double hydroxide
Ordered nanocomposite
Biomimetic
Self-assembly

ABSTRACT

A new generation of ordered, mineral-reinforced polymer nanocomposites is emerging for which assembly of platelets into planar-random array provides the reinforcement structure. Motivated by this goal, Co–Al layered double hydroxide (LDH) tactoids (diameter ~3 μm, thickness ~30 nm) were synthesized and their colloidal stability in water as a function of pH was characterized by sedimentation and zeta-potential measurements. The tactoids in both stable and unstable suspensions assembled into sheet materials with a layered planar random arrangement during filtration presenting a putative reinforcement structure. Exfoliated nanosheets, characterized by the disappearance of diffraction peaks in XRD patterns and by AFM, were also assembled and produced a region of 10 μm next to the filtration membrane which was highly ordered but in which the order reduced at further distances because of higher entropic undulation of very thin platelets at much reduced filtration rates. Reassembly of these exfoliated platelets confirmed that more ordered parallel structures are obtained with tactoids. Such structures resemble that of nacre and could serve as reinforcements for subsequent infiltration by matrix resins in the same way that carbon fibre woven mat is prepared for fibre reinforced polymers.

1. Introduction

There is a pervading view in the materials community that composite materials which emulate the layered bricks-and-mortar structure of nacre (mother of pearl) would deliver a combination of high elastic modulus and high work of fracture giving rise to high fracture toughness (K_{IC}) [1–3]. In selecting calcium salts for reinforcement of mollusc shells on the basis of availability and solubility, nature, faced with the very low toughness of aragonite (~1 MPa $m^{1/2}$), refined the microstructure to produce nacre with K_{IC} = 4–6 MPa $m^{1/2}$ using 5 vol.% organic material. Its toughness emerges in part from crack deviation along a tortuous path where energy is absorbed by the organic constituent, by platelet interlocking and by jamming due to platelet thickness variation [4–6]. This provides one of the best examples of the principle that underpins materials science that micro- and nano-structures have a commanding influence on properties [7–9]. In the laboratory, experiments using alumina and polymethylmethacrylate [9] have produced a composite with twenty times the toughness of either constituent simply by microstructural rearrangement of

* Corresponding author. Tel.: +44 020 7679 4689.
E-mail address: j.r.g.evans@ucl.ac.uk (J.R.G. Evans).

0927-7757/$ – see front matter © 2012 Elsevier B.V. All rights reserved.
http://dx.doi.org/10.1016/j.colsurfa.2012.05.033

two inherently brittle materials, a lively demonstration of the remarkable influence of microstructure on properties which is transforming strategic thinking in composite materials [10].

Renewed interest in the biomimetic 'copying' of the nacre structure emerges from the need to find composite materials with high strength and stiffness to weight ratio as replacements for carbon fibre composites, particularly in a new generation of low fuel consumption automotive applications where the high cost of carbon fibre is considered a threat to market penetration.

Recent work on the ordering of exfoliated platelets of montmorillonite in a polyvinyl alcohol matrix [11] and the resulting mechanical properties: tensile stress of 400 MPa and modulus of 106 GPa have given hope that the long term goal of mimicking the nacre microstructure with high volume fractions of an inexpensive and plentiful mineral reinforcement is now in sight. The assembly process used was layer-by-layer deposition in which 1800 dipping and drying operations are needed to produce a film that is 1.5 μm thick. Furthermore strength was measured on samples of 1.5 μm × 1 mm × 4–6 mm so that corrections are needed for the volume dependence of strength but the important point that has been established by that work is that high-strength composites from clays and polymers can be made. The question now is: how can these composites be made in sufficient volume to provide a viable manufacturing process? Previous work at Schlumberger research [12] suggested simple methods like filtration could be effective but did not study the resulting microstructure and our previous work [13] showed that thin layered structures of natural montmorillonite could be obtained by several approaches including filtration.

Clays are natural layered aluminosilicates with cations sandwiched between the layers. Layered double hydroxides (LDHs), also known as hydrotalcite clays, are also laminar minerals with anions sandwiched between hydroxide layers. LDHs are present in nature [14] and can be synthesized in the laboratory; synthetic LDHs have better-defined geometry and crystal structure than their natural counterparts. LDHs have the general formula $[M_{1-x}{}^{2+}M_x{}^{3+}(OH)_2]^{x+}[A_{x/n}{}^{n-}\cdot mH_2O]^{x-}$, where M^{2+} and M^{3+} are di- and tri-valent metallic cations and A^{n-} represent the anions in the interlayer space [15,16]. Al^{3+} ions are the main trivalent cations. Mg–Al [17] and Zn–Al [18] LDHs are the most commonly studied. Transition metal-bearing LDHs such as Co–Al [19,20], Fe–Al [21] and Ni–Al [22] may have special applications due to their magnetic, catalytic and optical properties. Zn–Al layered hydroxides function as photocatalysts for oxidation of phenol [23] and similar Mg–Al LDH have been arranged into thin films (∼1.5 μm) in conjunction with polysodium 4-styrenesulphonate using layer-by-layer (LBL) assembly [24]. Zn-, Mg- and Co-LDH were assembled into thin films by LBL and spin coating methods [25].

We synthesized Co–Al LDHs and adjusted the colloidal stability of their dispersions. We also prepared delaminated (exfoliated) LDH nanosheets by gradual ion exchange followed by redispersion in formamide. These were arranged by filtration on a 0.2 μm pore-size membrane to explore the effectiveness of this method for the assembly of planar random structures of platelets with different colloidal stability and platelet thickness.

2. Experimental details

2.1. Synthesis of LDH platelets

Co–Al LDH particles were synthesized based on a procedure [15] for producing platelets in the micrometer diameter region and with $CO_3{}^{2-}$ as the interlayer anions. Reactants consisting of 1.42 g $CoCl_2\cdot 6H_2O$, 0.72 g $AlCl_3\cdot 6H_2O$ and 1.26 g urea (obtained from Sigma Aldrich, Poole, Dorset, UK) were dissolved in 600 mL distilled water in a three-necked round bottom flask. The solution was purged with nitrogen gas for 5 min before being heated and refluxed for 48 h at 120 °C under nitrogen protection in an oil bath. The resulting particles were filtered and washed thoroughly with distilled water four times and redispersed to the initial concentration, which was measured to be 0.15 wt.% by gravimetric drying. All further experiments were derived from this stock dispersion designated LDH–$CO_3{}^{2-}$.

Ion exchange and exfoliation of the particles were carried out using modifications of previous methods [15] in which the platelets were never dried or ground. Typically 100 mL stock dispersion was filtered and redispersed into 100 mL mixture of NaCl (1 M) and HCl (3.3 mM) solution by vigorous shaking. This suspension was then mixed on a roller table for 24 h to exchange $CoCl_2\cdot 6H_2O$ for Cl^- and this product was designated as LDH–Cl^-. It was filtered and washed with distilled water four times, then redispersed into 100 mL $NaNO_3$ solution (0.1 M). This suspension was mixed for another 24 h and separated by the same method as LDH–Cl^- to produce LDH–$NO_3{}^-$. LDH–NO_3^- was then re-dispersed into 100 mL formamide and shaken vigorously and mixed on a roller table for 24 h to give a putative exfoliated LDH designated as E-LDH. Part of the E-LDH so produced was separated from formamide by centrifugation and re-dispersed in distilled water to produce re-assembled LDH.

2.2. Preparation of LDH films

In order to produce oriented LDH films, the appropriate dispersions were filtered in a disposable Nalgene filter funnel fitted with a sterile cellulose nitrate membrane of 0.2 μm pore size obtained from Thermo-Fisher Scientific (Leicestershire, UK). The filter cakes together with the filter membrane were carefully removed and dried for 24 h in air at room temperature and then in a vacuum oven at ambient temperature for 24 h. The E-LDH dispersion in formamide was filtered with a Millipore Fluoropore membrane made of hydrophilic PTFE and having the same pore size (obtained from Millipore, Hertfordshire, UK).

2.3. Characterisation methods

Part of the stock LDH–$CO_3{}^{2-}$ dispersion was diluted 10 times to 0.015 wt.% before adjusting pH with added hydrochloric acid or sodium hydroxide solutions. Zeta-potential and particle size were measured on a Zetasizer nano-ZS (Malvern Instruments, Malvern, UK) at 25 °C in clear disposable zeta cells. Sedimentation of the stock LDH–$CO_3{}^{2-}$ dispersions (0.15 wt.%) at different pH was recorded in optical quartz cells with a path length of 10 mm as a function of time. XRD measurements were run on either a Bruker AXS D4 Endeavor or a Bruker D500 Theta/2Theta diffractometer at ambient temperature. Scans were from 2 to 55° 2θ with 6 s counting time per step and 0.05° gap per step. SEM images were obtained on JEOL JSM-7401F. Samples were coated beforehand with a GATAN coater (Model 681) with a layer of Au 1–2 nm thick. AFM images were taken on a Veeco Dimension 3100 in tapping-mode and the images were analyzed with the Nanoscope v.6 software. Samples were deposited on freshly cleaved mica surfaces and dried in a nitrogen flow.

3. Results and discussion

3.1. Particle size analysis

After 11 ks (3 h) in the reaction vessel, the clear pink solution started to become turbid and a pink precipitate developed over the 48-h refluxing period. This precipitate, both in its as-prepared

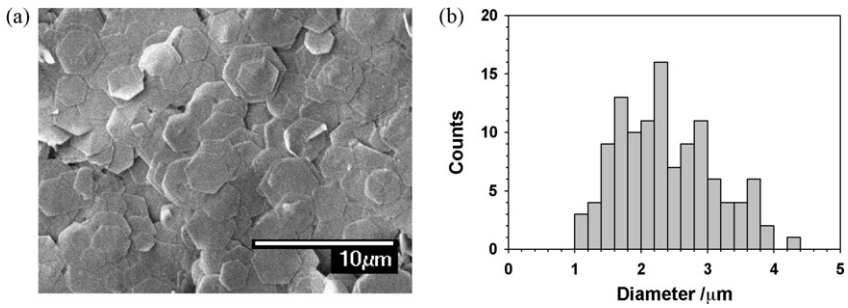

Fig. 1. (a) SEM image of the as-prepared Co–Al LDH particles and (b) the derived platelet diameter (distance between two opposite edges) distribution.

state and after washing, sedimented very quickly. Fig. 1(a) shows a scanning electron microscope image of the as-synthesized LDH particles and the number average diameter is 2.4 ± 0.07 μm as deduced from the analysis of SEM images (Fig. 1(b)). The Zetasizer gave a *z*-averaged diameter of 2.9 μm with a polydispersity index 0.56. The estimate from SEM images examines a limited sample area and the more reliable data is derived from the Zetasizer. The platelets were further characterized by AFM imaging and Fig. 2(a) shows a typical tapping-mode AFM image. The platelet thickness is in the region of 30 nm by section analysis across one edge of the platelet as shown in Fig. 2(b).

3.2. Stability of LDH dispersions as a function of pH

The colloidal stability of platelets in dispersion may influence the formation of ordered structures and according to previous research [26,27], flocculated systems may be unable to pack efficiently so the stability of the LDH platelets was investigated. The basal surfaces are positively charged due to isomorphous substitution of Co by Al while the charges on the edges arise from the hydroxyl groups and are pH-dependent. Hence they carry positive charges at lower pH due to the protonisation of the OH groups and are negatively charged at higher pH caused by the loss of protons [28]. As a result, it is possible to stabilize LDH platelets at lower pH due to the repulsion forces between particles carrying charges of the same sign on both basal and edge surfaces. They may however flocculate at higher pH due to the attractive interaction between the negatively charged edges and positively charged basal surfaces. In principle, this feature of LDHs is the reverse of clays whose basal surfaces are negatively charged [29] and which tend to aggregate at lower pH and *vice versa*.

Fig. 3 shows the zeta-potential of LDH particles in their dilute (0.015 wt.%) aqueous suspension as a function of pH. It can be seen that at pH 2 and 3, the potential is about +63 mV; as pH rises, the potential drops and turns negative at pH ∼10. Generally when the zeta potential is higher than +30 mV or lower than −30 mV, the dispersion is regarded as stable. This shows that the colloidal stability of LDH platelets is indeed pH-dependent and confirms that these platelets can be electrostatically stabilized at lower pH where the whole particle presents a high positive potential resulting from the combination of charges from the edges and the basal surfaces. On the contrary, at higher pH, the charge at the edges changes to negative and counteracts part of the positive charge of the basal surface; this manages to make the whole particle present a negative potential at pH ≥ 10. Furthermore the potential reached a plateau at pH 6.0–9.5 possibly caused by the amphiphilic property of Al–OH which acts as a buffering agent. The isoelectric point of these platelets is in the region pH 9–10. These properties for Co–Al LDH platelets can be compared to earlier work for Mg–Al LDH platelets which also reported that the electrophoretic mobility of Mg–Al LDH platelets is highly pH dependent, decreases as pH rises and reaches a plateau at pH 6.5–8.5 [30]. Based on these values it can be predicted that the dispersion should stay stable below pH 5 and start to flocculate above pH 6 and serious flocculation should occur at ∼pH 10.

The stability can be deduced from sedimentation tests as shown in Fig. 4. The dispersion at pH 3 represents the range where zeta-potential is higher than +30 mV; the dispersion at pH 7 is the original LDH suspension without additives and represents the medium range where zeta-potential is lower than +30 mV; the dispersion at pH 10 represents the range above the isoelectric point. The starting situation is represented by Fig. 4(a), 1 min being the time required to set up the vessels and camera. The suspension was most stable at pH 3 (corresponding to zeta-potential of +63 mV, Fig. 3) and particles flocculated at pH 7 and pH 10 (corresponding to −30 mV < zeta potential < +30 mV, Fig. 3). It can be seen that the particles flocculated seriously at pH 10 characterized by faster sedimentation and a loose sediment layer; the particles slightly flocculated at pH 7 and gave denser sediment and the particles at pH 3 are well dispersed and gave very dense sediment. This visual observation verifies the prediction based on the zeta-potential measurement.

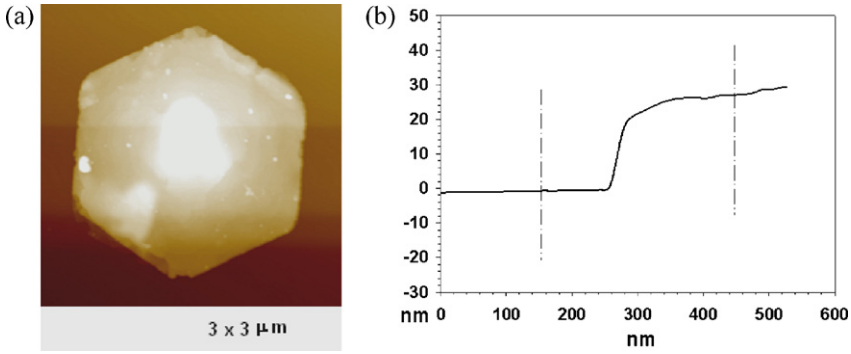

Fig. 2. (a) Tapping mode AFM image and (b) section analysis across an edge for an as-prepared Co–Al LDH particle.

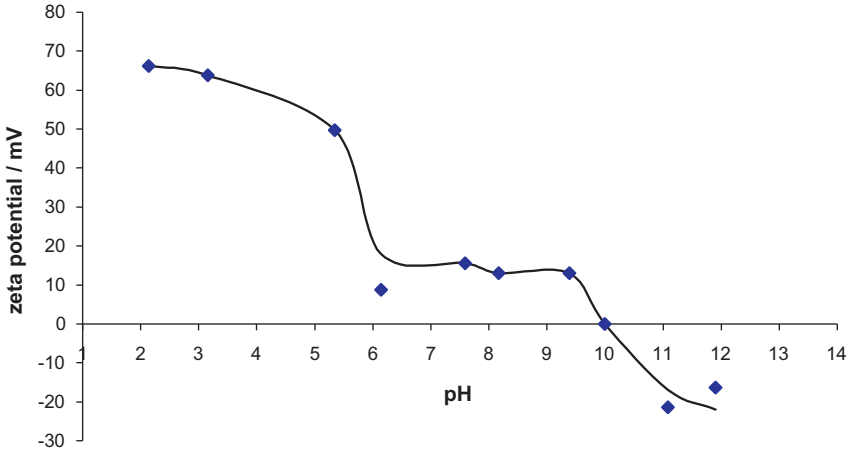

Fig. 3. Zeta-potential for LDH particles in its aqueous dispersion (0.015 wt%) as a function of pH.

3.3. LDH films obtained by filtration

Vacuum-assisted filtration through 0.2 μm porous cellulose membrane resulted in an average flux of 0.2 L m^{-2} s^{-1} or an average flow velocity of 200 μm s^{-1} overall. In some experiments, the vacuum was applied immediately (within 1–2 s) after filling the filtration vessel. In others, the contents of the filter vessel were left for 1 h before the vacuum was applied. The results of filtration experiments can therefore be interpreted in conjunction with the sedimentation results reported in Fig. 4. In the case of pH 3 suspensions, the extent of sedimentation over the 5 min needed to complete the filtration was minimal as deduced from (Fig. 4(b)) which shows the sedimentation state at 6 min. So these samples were assembled against the membrane in a flux of liquid with average velocity 200 μm s^{-1} rather than by sedimentation. On the other hand, the pH 3 suspensions left for 1 h had undergone significant sedimentation as judged by the sedimentation state at 1.5 h (Fig. 4(c)) before vacuum was applied because the flux in the filter without applied vacuum was negligible. For pH 10 suspensions, on the other hand, sedimentation had almost completed before the

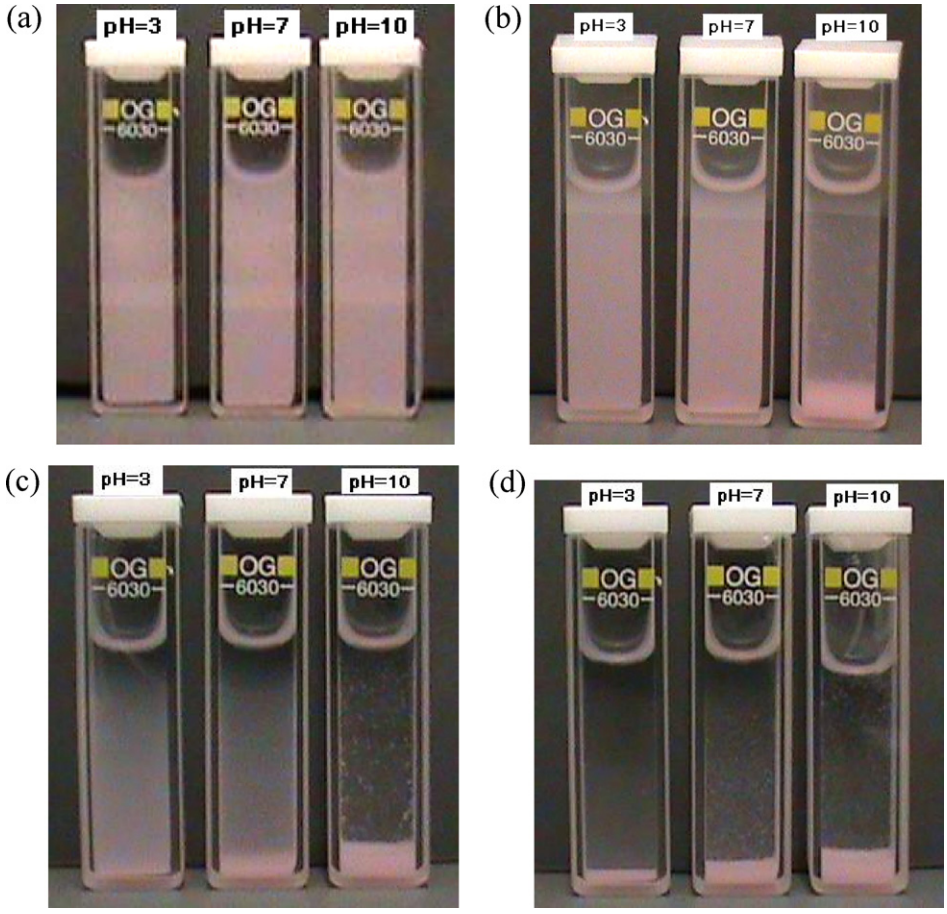

Fig. 4. Sedimentation records for LDH suspensions at pH 3, 7 and 10 after (a) t = 60 s (1 min); (b) t = 360 s (6 min); (c) t = 5400 s (1.5 h) and (d) t = 72 ks (20 h).

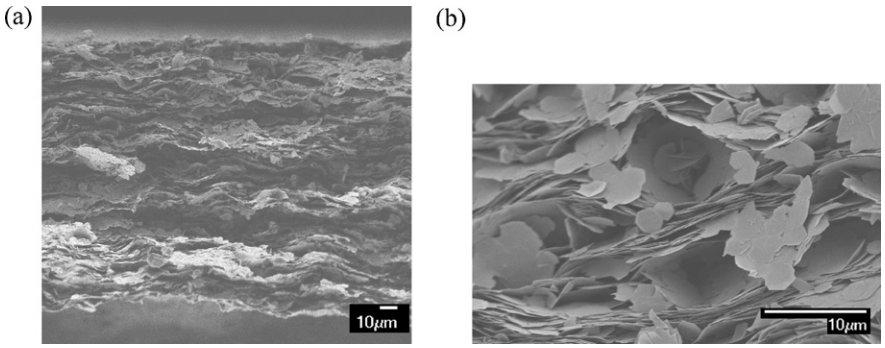

Fig. 5. SEM images of the cross-section of the LDH film obtained by filtering the pH = 3 dispersion at (a) lower magnification showing a layered assembly and (b) higher magnification showing defects thought to arise from entrapped bubbles.

vacuum was applied (Fig. 4b and c) in both cases. The sediment however is loose and characteristic of a partially flocculating system so that the morphology of the deposit can still be modified by compaction against the filter membrane once vacuum is applied as shown below.

Fig. 5 shows the typical SEM images for the cross-section of the filter cake resulting from LDH suspension at pH 3, which is the most stable dispersion. It was prepared by vacuum-assisted filtration and the vacuum pump connected to the filter was turned on immediately after the dispersions were transferred to the filter funnels. Samples that were allowed to sediment for 1 h and then filtered produced alignment in the resulting structure that was similar to that shown in Fig. 5(a).

Although there is evidence of overall preferred in-plane orientational alignment of the platelets, a significant degree of disorder was found. This takes two forms: hollow regions surrounded by a local 'house of cards' structure (Fig. 5(b)) and waviness in the structure which appears to be replicated throughout the assembly once an alignment defect has been introduced at an earlier stage. Thus the microstructure is characterized by a trend to form a layered structure interrupted by defects which then propagate waves.

Closer observation of the holes (Fig. 5(b)) indicates hollow spheres surrounded by deformed platelet shells which may have resulted from air bubbles with platelets attached parallel to the liquid-air interface before filtration. The original bubbles would be in the 10–20 μm region and therefore have low upthrust. Indeed a large number of air bubbles formed while stirring/shaking the dispersions during the synthesis and processing of the dispersions. This was initially ignored because it was assumed (wrongly) that the viscosity was low enough for air bubbles formed during mixing to be released when the mixing stopped. Nevertheless, opacity made it hard to tell by visual observation whether the entrapped air had been released and so vacuum degassing of the dispersions was carried out.

Fig. 6(a) and (b) show the cross-sections of samples with the same pH = 3 as those shown in Fig. 5, but degassed before filtration. The alignment of the platelets was greatly improved and the packing efficiency has increased. The local 'house of cards' structures have gone and the waviness has been reduced considerably. This high degree of ordering produced by such a simple operation compared to the layer-by-layer process provides encouragement that a new generation of nacre-like composites can be produced on a commercial scale.

It is particularly interesting that the flocculated particles at pH 10 seen in the sedimentation experiment (Fig. 4) were also successfully aligned by filtration. The aggregated particles in the loosely flocculated arrangements are assumed to adopt a 'house-of-cards' structure in suspension due to the attraction between the edges and the basal surfaces [28], an effect widely associated with platelet minerals [31]. That they also produced a layered structure means that such assemblies are easily broken down when the suspension is filtered.

Several factors influence the alignment of platelets during vacuum-assisted filtration: the flow of water, gravity and pressure

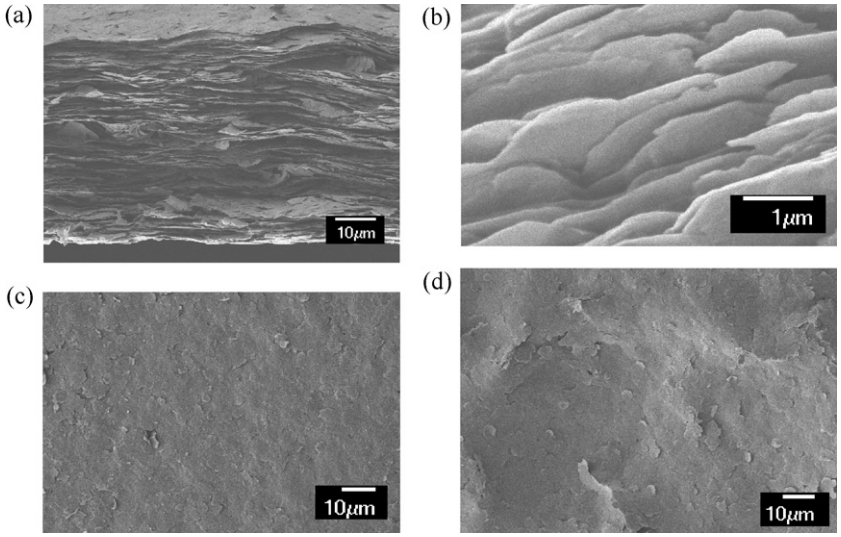

Fig. 6. SEM images of the LDH film obtained by filtering the degassed dispersion of pH 3: the cross-section at (a) lower magnification and (b) higher magnification, the lower surface (c) and the upper surface (d).

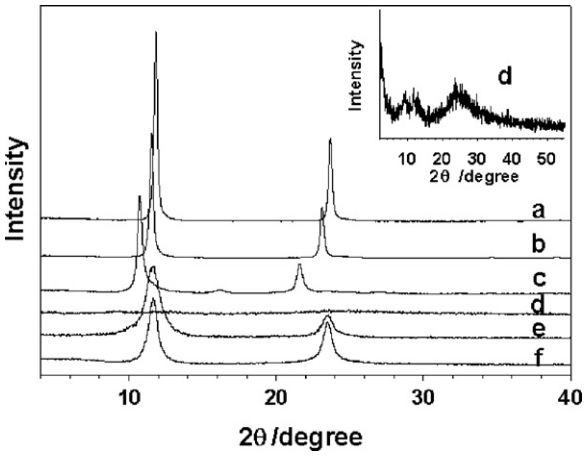

Fig. 7. XRD patterns of (a) LDH–CO_3^{2-}, (b) LDH–Cl^-, (c) LDH–NO_3^-, (d) exfoliated LDH paste in formamide, (e) dried exfoliated LDH paste in formamide and (f) re-assembled LDH by re-dispersion of exfoliated LDH in water. The inserted graph is the expanded pattern for exfoliated LDH-formamide paste.

gradient. The flow direction of water is perpendicular to the plane of the filter membrane and in laminar flow with low Reynold's number, the platelets would tend to align parallel to the flow direction. This orientation is changed by the torque applied to each platelet by the filtrate as it touches the filter cake and in this case, the torque on a platelet caused by water flow during filtration forces the basal surface to attach to the surface below. This effect is reinforced by gravity and appears sufficient to overcome the weaker flocculating attraction between the LDH particles.

The lower surfaces as shown in Fig. 6(c) are made up of particles deposited in the fastest flow on the fresh membrane and are nearly perfectly flat with few defects. There is a tendency for defects to be replicated and magnified as the film develops, so the top surfaces of the filter cakes are somewhat wavy (Fig. 6(d)) caused by the propagation of alignment defects inside the film although the platelets still tend to assemble flat.

3.4. Exfoliation of LDH platelets and alignment of exfoliated LDH

Fig. 7 shows the XRD patterns of the LDH particles with different interlayer anions. Fig. 7(a) shows the as-synthesized LDH containing CO_3^{2-}; (b) and (c) are for the Cl^-- and NO_3^--exchanged LDH platelets respectively. The inter-planar spacing derived from the diffraction peaks are listed in Table 1. It can be seen that the LDH platelet swells when CO_3^{2-} ions are replaced by Cl^-. Data for CO_3^{2-} (0.75 nm) and Cl^- (0.77 nm) exchanged LDH are similar to the values previously obtained for this system [15]. The basal interlayer spacing becomes even greater (0.86 nm) when NO_3^- ions are substituted for Cl^-, indicating that the basal plane spacing increases in the counter-ion order: $CO_3^{2-} < Cl^- < NO_3^-$ and this also confirms the effectiveness of ion exchange. The interlayer spacing of LDH–NO_3^- in our work is slightly lower than the value (0.89 nm) in references [15] and [32] possibly because a small proportion of the interlayer spaces are occupied by CO_3^{2-} contributed by the ionization of carbon dioxide dissolved in the distilled water used. Li et al. managed to reassemble the exfoliated Mg–Al LDH platelets to give the interlayer distance typical of its nitrate form by using nitrogen protection and deionised water in the whole process [32].

After ion exchange, NO_3^- substituted LDH was redispersed into formamide and shaken vigorously. The resulting dispersion remained stable for several days. Part of the dispersion was then separated from formamide by centrifugation and the sediment was in the nature of a paste which was assessed by X-ray diffraction. Fig. 7(d) shows the XRD pattern of the exfoliated-LDH formamide paste. The diffraction peak disappeared and this means the platelets are exfoliated into single sheets. The significant halo around 24° of 2θ is attributed to the scattering of formamide [15]. The exfoliation is confirmed by the tapping-mode AFM image as shown in Fig. 8. A thickness of ~1 nm is derived by section analysis across the edges of the nanosheets (see Fig. 8(b)). AFM images also disclose that the exfoliated system still contains a few incompletely exfoliated platelets with almost the same thickness as the original platelets (~30 nm). A small population of unexfoliated particles or reassembled platelets caused the very small peak at around 12° in the XRD patterns (Fig. 7(d)). This shows that the slightly narrower interlayer space caused by the contamination of CO_3^{2-} in LDH–NO_3^- did not undermine the exfoliation. It is common to find that the extent of exfoliation of platelets rarely reaches 100% and this degree of exfoliation of LDH was accepted without further effort to extend it. The paste was allowed to dry in a vacuum oven and the basal spacing did not return to the value for LDH–NO_3^- as expected because of the continued capture of CO_3^{2-} ions from dissolved CO_2.

The suspension was filtered and it took 3 ks to filter 60 mL suspension compared to the unexfoliated suspensions which took ~300 s; an effect associated with the lower permeability that develops in the exfoliated filter cake. Fig. 9(a) and (b) shows respectively the lower surface and cross-section of the film obtained in this way. As most of the platelets became substantially thinner which is revealed by the AFM images and the XRD data showing exfoliation of the platelets, SEM could hardly discern their edges (Fig. 9(a)). Fig. 9(b) shows that the platelets are ordered in the region next to the filter membrane to a thickness of ~10 μm and packed less

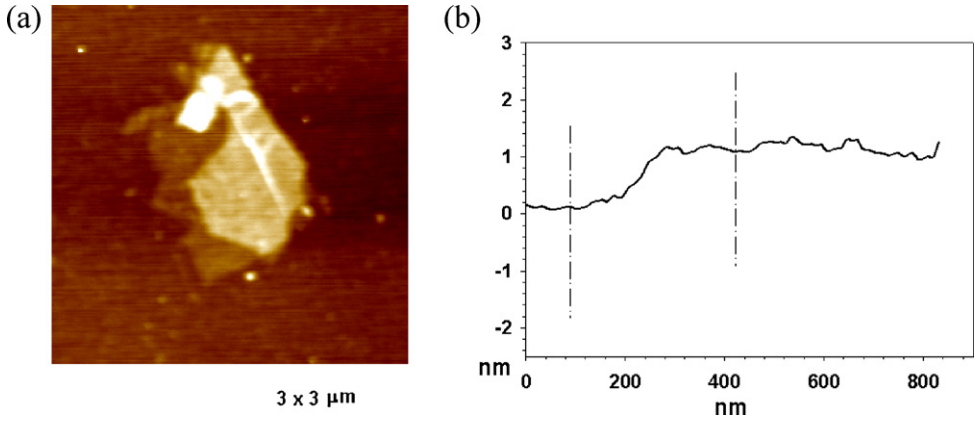

Fig. 8. Tapping-mode AFM image (a) and section analysis (b) of exfoliated LDH nanosheets deposited on freshly cleaved mica.

Table 1
Interlayer spacing for LDH particles with different interlayer counter ions and in different liquids (the fundamental *d*-spacings were the same for 1st and 2nd order reflections).

	LDH–CO_3^{2-}	LDH–Cl^-	LDH–NO_3^-	Dried formamide-LDH	Formamide-LDH, reassembled in water
d-Spacing (nm)	0.75	0.77	0.86	0.78	0.76

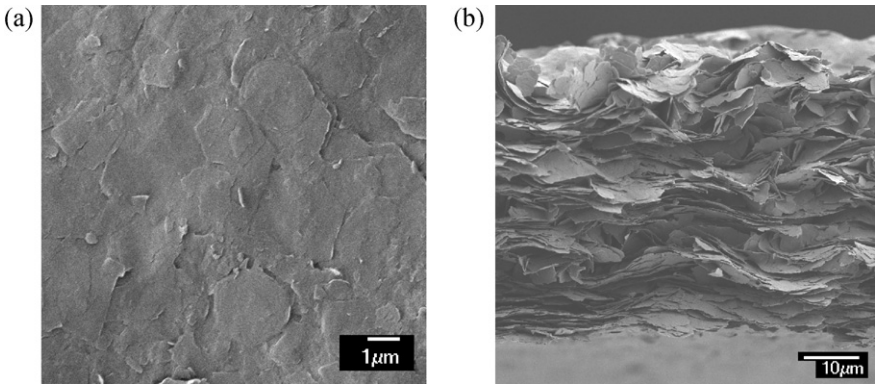

Fig. 9. SEM images of a film obtained by filtering the formamide suspension of exfoliated LDH particles: (a) bottom surface and (b) cross-section.

efficiently further away. Isotropic to liquid crystal-like phase transitions are reported for LDH in suspension and can be extended by organic adsorbents [33]: the coalescence of such structures could also contribute to disordered regions. It is likely that the first few ordered layers control the permeability of the entire cake. To exclude the hypothesis that the platelets did not pack efficiently because the suspension was too crowded, the same volume of suspension was diluted 10 times and filtered but it resulted in a film with the same structure showing no improvement. As these single sheets are very thin and less rigid, they easily deform. Indeed recent work confirms that undulations spontaneously form in single sheets of montmorillonite [34], graphene [35], and layered double hydroxide [36]. In the upper region, the lower pressure difference experienced by the nanosheets and the deceased flow rate of formamide caused by the build-up of the first layers of the filter cake lead to less torque on each plate; this, combined with naturally occurring undulation inhibits a highly ordered structure.

The deflection, y of a flat plate is proportional to $1/t^3$ where t is the thickness [37], so the number of sheets in a tactoid has a very strong influence on its ability to undulate and bend during assembly. This explains why LDH tactoids could be assembled into highly ordered arrangements but exfoliated nanosheets showed more disorder. The lower effectiveness of the filtration method in assembling layered nanosheets of this LDH is thus partly dependent on the extent of exfoliation and the large aspect ratio. The in-plane Young's modulus for LDH platelets from molecular dynamic simulation [36] is 63.4 ± 0.5 GPa for a hydrated system and 139 ± 1 GPa for the LDH sheets alone. This is 60% of that of montmorillonite clay platelets, calculated to be 230 GPa by the same method [34]. Both minerals provide substantial modulus enhancement for polymer matrices which typically have Young's Moduli in the 1–3 GPa region and so both minerals are competitors for the role of reinforcing agents in ordered platelet composites. The easier processing of LDH, resulting particularly from its reduced tendency to form gels, might compensate for its lower modulus. The dispersion medium may also affect the assembly because it has an impact on the van der Waals interaction between the platelets. For example, exfoliated clay nanosheets dispersed in water can be assembled into a sufficiently ordered film by filtration [38]. Graphene has superb mechanical strength and up to 20 μm thick films with a layered structure have been made [39,40]. There is an argument therefore to suggest that the assembly of Co–Al LDH tactoids instead of exfoliated nanosheets may produce a more ordered structure overall.

It has been reported that Co–Al LDH platelets, which have been exfoliated in formamide, re-assemble when they are re-dispersed into water [15]. This enables us to test the effect of platelet rigidity on the degree of order in the resulted film: it should be influenced by the degree of reassembly. A filter-cake was therefore prepared from platelets which had been re-assembled by re-dispersion in water. Their XRD pattern (Fig. 7(f)) confirmed the reassembly of the exfoliated sheets with a *d*-spacing 0.76 nm, which is slightly higher than the as synthesized LDH–CO_3^{2-} (0.75 nm) due to the continued capture of CO_3^{2-} in water. Fig. 10 shows the cross-section of the

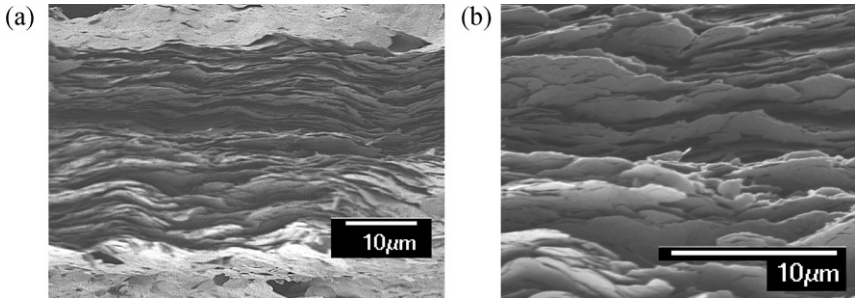

Fig. 10. SEM images of the cross-section from the filter cake of re-assembled LDH by re-dispersion of exfoliated LDH in water at (a) lower magnification and (b) higher magnification.

film obtained by filtration of this suspension and it is clearly much more ordered than that from the exfoliated LDH platelets.

4. Conclusions

Co–Al LDH tactoids (diameter: ~2.9 μm; thickness: ~30 nm) were synthesized in aqueous suspensions: they dispersed well at lower pH but aggregated at higher pH. This is because the platelet basal surface carries positive charges due to the isomorphous substitution of Co atoms by Al atoms and the platelet edge carries positive charges at lower pH and negative charges at higher pH. The IEP of its surface was found to be between pH 9–10. The well-dispersed and the aggregated platelets could both be aligned to form a layered structure by the filtration method, which indicates that the flow processes in filtration can overcome the weaker aggregation forces. The dispersion needs to be degassed in order to produce a higher degree of order by removing the relics of entrapped microbubbles.

The tactoids synthesized in this way were exfoliated by formamide after gradual substitution of the interlayer ions; XRD confirmed the expected basal plane spacings of the substituted LDHs. The single nanosheets packed very efficiently in the region close (~10 μm) to the filter membrane when the flow rate was at maximum but the packing became less regular further from the filter because of flexibility of the nanosheets combined with the reduced flow rate and pressure difference encountered after the built-up of the first layers of filter cake. The platelets were then reassembled into tactoids and the ordered structure resulting from the reassembled platelets confirms that the tactoid rigidity plays a part in forming ordered packing arrangements in filtration processes. LDH, montmorillonite and graphene are all competitors for the role of platelet reinforcements in ordered polymer nanocomposites. LDH may have advantages in terms of ease of processing and conferment of fire-resistance.

Acknowledgments

The authors are grateful for Engineering and Physical Sciences Research Council funding under Grant No: EP/H048855/1. "The Clay Aeroplane". Thanks to Dr Richard Thorogate (London Center of Nanotechnology, UCL) for AFM imaging, Mr. Mark Turmaine (Bioscience, UCL) for SEM imaging and Mr. Martin Vikers (Chemistry, UCL) for help on XRD.

References

[1] D.L. Kaplan, Mollusc shell structures: novel design strategies for synthetic materials, Curr. Opin. Solid State Mater. Sci. 3 (1998) 232–236.
[2] A.P. Jackson, J.F.V. Vincent, R.M. Turner, Comparison of nacre with other ceramic composites, J. Mater. Sci. 25 (1990) 3173–3178.
[3] B. Richter, S. Kellner, H. Menzel, P. Behrens, B. Denkena, S. Ostermeier, C. Hurschler, Mechanical characterization of nacre as an ideal-model for innovative new endoprosthesis materials, Arch. Orthop. Trauma Surg. 131 (2010) 191–196.
[4] E. Munch, M.E. Launey, D.H. Alsem, E. Saiz, A.P. Tomsia, R.O. Ritchie, Tough, bio-inspired hybrid materials, Science 322 (2008) 1516–1520.
[5] K.S. Katti, D.R. Katti, Why is nacre so tough and strong? Mater. Sci. Eng. C 26 (2006) 1317–1324.
[6] F. Barthelat, Nacre from mollusk shells: a model for high-performance structural materials, Bioinsp. Biomim. 5 (2010) 035001.
[7] F. Song, Y.L. Bai, Effects of nanostructures on the fracture strength of the interfaces in nacre, J. Mater. Res. 18 (2003) 1741–1744.
[8] S. Veprek, A.S. Argon, R.F. Zhang, Design of ultrahard materials: Go nano!, Philos. Mag. 90 (2010) 4101–4115.
[9] B.J. Ash, R.W. Siegel, L.S. Schadler, Mechanical behavior of alumina/poly(methyl methacrylate) nanocomposites, Macromolecules 37 (2004) 1358–1369.
[10] R.O. Ritchie, The conflicts between strength and toughness, Nat. Mater. 10 (2011) 817–822.
[11] P. Podsiadlo, A.K. Kaushik, E.M. Arruda, A.M. Waas, B.S. Shim, J. Xu, H. Nandivada, B.G. Pumplin, J. Lahann, A. Ramamoorthy, N.A. Kotov, Ultrastrong and stiff layered polymer nanocomposites, Science 318 (2007) 80–83.
[12] P.V. Coveney, M. Watkinson, A. Whiting, E.S. Boek, Method for stabilizing clayey geological formations surrounding hydrocarbon wells, and method for drilling a well bore into potentially hydrocarbon-bearing formations, World Patent WO 9931353, 1999.
[13] T. Liu, B. Chen, J.R.G. Evans, Ordered assemblies of clay nano-platelets, Bioinsp. Biomim. 3 (2008) 016005.
[14] S.V. Krivovichev, V.N. Yakovenchuk, E.S. Zhitova, A.A. Zolotarev, Y.A. Pakhomovsky, G.Y. Ivanyuk, Crystal chemistry of natural layered double hydroxides, Mineral. Mag. 74 (2010) 821–832.
[15] Z. Liu, R. Ma, M. Osada, N. Iyi, Y. Ebina, K. Takada, T. Sasaki, Synthesis, anion exchange, and delamination of Co–Al layered double hydroxide: assembly of the exfoliated nanosheet/polyanion composite films and magneto-optical studies, J. Am. Chem. Soc. 128 (2006) 4872–4880.
[16] X. Ma, H. Li, G. Zhua, L. Kanga, Z.-H. Liu, Hydrothermal preparation and anion exchange of Co^{2+}–Ni^{2+}–Fe^{3+} $CO_3{}^{2-}$ LDHs materials with well regular shape, Colloids Surf. A: Physicochem. Eng. Aspects 371 (2010) 71–75.
[17] B. Pradhan, S.K. Srivastava, R. Ananthakrishnan, A. Saxena, Preparation and characterization of exfoliated layered double hydroxide/silicone rubber nanocomposites, J. Appl. Polym. Sci. 119 (2011) 343–351.
[18] F. Cao, Y. Wang, Q. Ping, Z. Liao, Zn–Al–NO_3-layered double hydroxides with intercalated diclofenac for ocular delivery, Int. J. Pharm. 404 (2011) 250–256.
[19] D.-Y. Wang, A. Das, F.R. Costa, A. Leuteritz, Y.-Z. Wang, U. Wagenknecht, G. Heinrich, Synthesis of organo cobalt–aluminum layered double hydroxide via a novel single-step self-assembling method and its use as flame retardant nanofiller in PP, Langmuir 26 (2010) 14162–14169.
[20] H. Peng, Y. Han, T. Liu, W.C. Tjiu, C. He, Morphology and thermal degradation behavior of highly exfoliated CoAl-layered double hydroxide/polycaprolactone nanocomposites prepared by simple solution intercalation, Thermochim. Acta 502 (2010) 1–7.
[21] R. Chitrakar, Y. Makita, A. Sonoda, T. Hirotsu, Fe–Al layered double hydroxides in bromate reduction: synthesis and reactivity, J. Colloid Interface Sci. 354 (2011) 798–803.
[22] V. Prevot, C. Forano, A. Khenifi, B. Ballarin, E. Scavetta, C. Mousty, A templated electrosynthesis of macroporous NiAl layered double hydroxides thin films, Chem. Commun. 47 (2011) 1761–1763.
[23] A. Patzkó, R. Kun, V. Hornok, I. Dékány, T. Engelhardt, N. Schall, Zn–Al layer hydroxides as photocatalysts for oxidation of phenol in aqueous solution, Colloids Surf. A 265 (2005) 64–72.
[24] V. Hornok, A. Erdohelyi, I. Dékány, Preparation of ultrathin membranes by layer-by-layer deposition of layered double hydroxide (LDH) and polystyrene sulfonate (PSS), Colloid. Polym. Sci. 283 (2005) 1050–1055.
[25] T. Aradi, V. Hornok, I. Dékány, Layered double hydroxides for ultrathin hybrid film preparation using layer-by-layer and spin coating methods, Colloids Surf. 319 (2008) 116–121.
[26] T.H. Lin, W.H. Huang, I.K. Jun, P. Jiang, Bioinspired assembly of colloidal nanoplatelets by electric field, Chem. Mater. 21 (2009) 2039–2044.
[27] F. Bennadji-Gridi, A. Smith, J.-P. Bonnet, Montmorillonite based artificial nacre prepared via a drying process, Mater. Sci. Eng. B 130 (2006) 132–136.
[28] J.A. Gursky, S.D. Blough, C. Luna, C. Gomez, A.N. Luevano, E.A. Gardner, Particle-particle interactions between layered double hydroxide nanoparticles, J. Am. Chem. Soc. 128 (2006) 8376–8377.
[29] M.J. Avena, C.P. De Pauli, Proton adsorption and electrokinetics of an Argentinean montmorillonite, J. Colloid Interface Sci. 202 (1998) 195–204.
[30] G. Lagaly, O. Mecking, D. Penner, Colloidal magnesium aluminum hydroxide and heterocoagulation with a clay mineral. I. Properties of colloidal magnesium aluminum hydroxide, Colloid. Polym. Sci. 279 (2001) 1090–1096.
[31] C.C. Su, Y.H. Shen, Preparation and dispersive behaviors of reduced charge smectite, Colloids Surf. A: Physicochem. Eng. Aspects 259 (2005) 173–177.
[32] L. Li, R. Ma, Y. Ebina, N. Iyi, T. Sasaki, Positively charged nanosheets derived via total delamination of layered double hydroxides, Chem. Mater. 17 (2005) 4386–4391.
[33] W. Zhu, D. Sun, S. Liu, N. Wang, J. Zhang, L. Luan, Multiphase coexistence in colloidal dispersions of positively charged layered double hydroxides, Colloids Surf. A: Physicochem. Eng. Aspects 301 (2007) 106–112.
[34] J.L. Suter, P.V. Coveney, H.C. Greenwell, M.-A. Thyveetil, Large-scale molecular dynamics study of montmorillonite clay: emergence of undulatory fluctuations and determination of material properties, J. Phys. Chem. C 111 (2007) 8248–8259.
[35] A. Fasolino, J.H. Los, M.I. Katsnelson, Intrinsic ripples in graphene, Nat. Mater. 6 (2007) 858–861.
[36] M.A. Thyveetil, P.V. Coveney, J.L. Suter, H.C. Greenwell, Emergence of undulations and determination of materials properties in large-scale molecular dynamics simulation of layered double hydroxides, Chem. Mater. 19 (2007) 5510–5523.
[37] R.J. Roark, Formulas for Stress and Strain, 2nd ed., New York, McGraw Hill, 1943, p. 190.
[38] A. Walther, I. Bjurhager, J.-M. Malho, J. Pere, J. Ruokolainen, L.A. Berglund, O. Ikkala, Large-area, lightweight and thick biomimetic composites with superior material properties via fast, economic, and green pathways, Nano Lett. 10 (2010) 2742–2748.
[39] J. Gao, F. Liu, N. Ma, Z.-Q. Wang, X. Zhang, Environment-friendly method to produce graphene that employs vitamin C and amino acid, Chem. Mater. 22 (2010) 2213–2218.
[40] K.W. Puts, O.C. Compton, M.J. Palmeri, S.B.T. Nguyen, L.C. Brinson, High-nanofiller-content graphene oxide–polymer nanocomposites via vacuum-assisted self-assembly, Adv. Funct. Mater. 20 (2010) 3322–3329.